

# RSC Advances



This is an *Accepted Manuscript*, which has been through the Royal Society of Chemistry peer review process and has been accepted for publication.

*Accepted Manuscripts* are published online shortly after acceptance, before technical editing, formatting and proof reading. Using this free service, authors can make their results available to the community, in citable form, before we publish the edited article. This *Accepted Manuscript* will be replaced by the edited, formatted and paginated article as soon as this is available.

You can find more information about *Accepted Manuscripts* in the [Information for Authors](#).

Please note that technical editing may introduce minor changes to the text and/or graphics, which may alter content. The journal's standard [Terms & Conditions](#) and the [Ethical guidelines](#) still apply. In no event shall the Royal Society of Chemistry be held responsible for any errors or omissions in this *Accepted Manuscript* or any consequences arising from the use of any information it contains.

# Determination of potential main sites of apixaban binding in human serum albumin by combined spectroscopic and docking investigations

Qing Wang, Qiaomei Sun, Peixiao Tang, Bin Tang, Jiawei He, Xiaoli Ma, Hui Li\*

**Abstract:** Apixaban (AP, Eliquis<sup>®</sup>) is a novel pyrazole-based direct factor Xa inhibitor. This oral drug was developed by Bristol-Myers Squibb and Pfizer to treat and prevent thrombotic disorders. The single crystallographic data of AP were obtained with methanol as a solvent and classified as Form N-1. The interaction of AP with human serum albumin (HSA) was investigated via different spectroscopic techniques and molecular modeling. Fluorescence quenching between AP and HSA was observed to be a static process. Complexation by AP was the primary factor influencing decreases in the fluorescence intensity of HSA. AP fluorescence also decreased by approximately 20%. H-bonding and van der Waals forces played major roles in AP–HSA binding. Displacement experiments and molecular docking results demonstrated that the AP-binding site is mainly found in site 1 of HSA. The effect of AP binding on HSA esterase-like activity also confirmed this binding site. Three-dimensional fluorescence and circular dichroism studies showed that AP exerts minimal effects on the local conformation of HSA. This study provides useful information with which to better understand the utilization of AP.

## 1. Introduction

Venous thromboembolism (VTE) is a common vasculature disease with two clinical manifestations: deep vein thrombosis and pulmonary embolism.<sup>1, 2</sup> For decades, clinicians exclusively used intravenous or subcutaneous unfractionated heparin and oral vitamin K antagonists for VTE prophylaxis.<sup>3</sup> Recently, however, subcutaneous low-molecular-weight heparins and fondaparinux, which is a factor Xa (FXa) inhibitor, were developed.<sup>4</sup> Apixaban (AP, Eliquis<sup>®</sup>) is a novel oral pyrazole-based direct FXa inhibitor; this drug was developed by Bristol-Myers Squibb and Pfizer to treat and prevent thrombotic disorder.<sup>5, 6</sup> Since May 2011, AP has been approved for VTE prevention in adult elective hip or knee replacement patients in various countries, such as the USA, China, Brazil, Australia, New Zealand, and some European countries.<sup>3</sup> FXa inhibition enhances thrombin inhibition; thus, FXa inhibitors present better tolerability profiles than conventional antithrombotic medications, such as warfarin (WF).<sup>7–9</sup> AP inhibits FXa by binding to its FXa active site; the formation of this complex is reversible and highly selective.<sup>10</sup> AP is relatively bioavailable, reaches peak concentrations at approximately 3 h after administration, and presents a half-life of approximately 12 h.<sup>11, 12</sup> Physicians generally recommend that AP be orally administered twice daily to reduce peak-to-trough drug level

*College of Chemical Engineering, Sichuan University, Chengdu 610065, People's Republic of China. E-mail: lihuilab@sina.com; Fax: +86 028 85401207; Tel: +86 028 85405149.*

fluctuations and achieve less bleeding than that observed with once-daily anticoagulant treatment.

Human serum albumin (HSA), one of the most abundant blood plasma proteins, binds and transports several exogenous and endogenous substances; it also performs a key function in various biological systems and processes.<sup>13</sup> The protein has multiple hydrophobic binding sites that can bind to a diverse set of drugs.<sup>14, 15</sup> Drugs in the bloodstream can extensively and reversibly bind to HSA.<sup>16, 17</sup> In pharmacology, protein interactions can affect the biological activity and toxicity of drugs. AP binds to serum proteins *in vitro* (87%) and in serum obtained from humans receiving the drug (93%); the drug also displays a greater degree of binding to albumin than to  $\alpha$ -acid glycoprotein *in vitro* (66% vs. 9%).<sup>4</sup> However, details of this binding (e.g., binding mechanism, binding site, etc.) have not been reported.

In the present work, several spectroscopic molecular and docking methods were performed to investigate AP–HSA interactions. Prior to these techniques, crystalline AP was obtained and analyzed by single crystal X-ray diffraction. Previous studies have reported the polycrystalline phenomena and basic cell parameters of AP,<sup>18–21</sup> but a discussion on its stereochemistry is not yet available. The present study is necessary to improve the current understanding of the characteristics of AP at the atomic level. Fluorescence spectrometry was used to determine the AP–HSA binding affinity and investigate the interaction thermodynamics. Various molecular interactions can decrease fluorescence; thus, we focused on the main causes of AP-induced decreases in HSA fluorescence. Displacement and molecular docking techniques are useful methods to establish the main binding site on HSA because this molecule exhibits multiple hydrophobic binding sites, and two primary sites (1 and 2) are known key determinants of binding specificity.<sup>22, 23</sup> We utilized the esterase-like activity of HSA to verify the effect of AP on site 2. Drug–protein binding may affect the conformation and stability of the same protein; thus, three-dimensional (3D) fluorescence and circular dichroism (CD) studies were performed. The results of this study may provide valuable information on the mechanism and location of AP binding to HSA.

## 2. Materials and methods

### 2.1. Preparation of stock solution

Fatty acid-free HSA (A1887) with an assumed molecular weight of 66 500 g/mol was purchased from Sigma-Aldrich (St. Louis, USA) and used without further purification. Stock solutions (20.0  $\mu$ M) were prepared in Tris-HCl buffer (pH 7.40) and 0.1 M NaCl. AP (A726700), WF (W498500), phenylbutazone (PB; P1686), and ibuprofen (IB; 77519) were purchased from J&K Scientific, Ltd. (Beijing, China). AP, WF, PB, and IB were dissolved in anhydrous ethanol to obtain 2.0 mM stock solutions, which were then stored at 0–4 °C until use.

### 2.2 Materials and equipment

Fluorescence analyses were conducted on a Cary Eclipse fluorescence spectrophotometer (Varian, USA) equipped with a 1 cm quartz cell. Fluorescence spectra were obtained at 301, 310, and 318 K, whereas other fluorescence analyses were performed at 301 K and pH 7.40. AP shows good stability under these conditions. Fluorescence spectra were measured with 10/5 nm (excitation/emission)

slit widths unless otherwise specified.

Fluorescence lifetime measurements were obtained by time-correlated single photon counting (TCSPC) with a Horiba Jobin Yvon FluoroMax-4 spectrofluorometer (Horiba, France).

AP absorption and the effects of AP binding on the catalytic activity of HSA toward p-NPA were analyzed with a TU-1901 UV-vis spectrophotometer (Persee, Beijing, China) at room temperature.

CD spectra were recorded on a CD spectrometer (Model 400, AVIV, USA). The spectra were obtained at 298 K in a 2 mm quartz cell from 200 nm to 250 nm with a step size of 1 nm, a band width of 1 nm, and an average time of 0.5 s.

To evaluate the effect of ethanol on the HSA conformation and fluorescence quenching, 2.0  $\mu\text{M}$  HSA with 1.2% (v/v) ethanol was compared with free HSA by UV-vis, fluorescence, and CD spectroscopy. No clear changes were observed in the spectral profiles obtained (Fig. S1), which indicates that the HSA conformation does not change in the presence of 1.2% (v/v) ethanol. Thus, HSA structural changes were insignificant under the ethanol volume employed in this work. In this study, all fluorescence intensities were corrected for the absorption of excited light and the reabsorption of emitted light. The following relationship was used to correct the inner-filter effect:<sup>24</sup>

$$F_{\text{corr}} = F_{\text{obs}} \times e^{\frac{A_{\text{ex}} + A_{\text{em}}}{2}} \quad (1)$$

where  $F_{\text{corr}}$  and  $F_{\text{obs}}$  are the corrected and observed fluorescence intensities, respectively, and  $A_{\text{ex}}$  and  $A_{\text{em}}$  are the absorption values of the system at the excitation and emission wavelengths, respectively.

### 2.3. Molecular modeling preparation

Discovery Studio 3.1 (DS 3.1; Accelrys Co., Ltd., US) was provided by the State Key Laboratory of Biotherapy (Sichuan University, China). HSA crystal structures were obtained from a protein data bank (PDB) for docking simulations; the HSA PDB IDs were 2BXC and 2BXG, and both IDs were two-chained. 2BXC contains only PB, whereas 2BXG contains only IB.<sup>25</sup> Chain B was deleted from 2BXC and 2BXG. Hybridization states, charges, and angles were then assigned to the protein structure with missing bond orders. Explicit H atoms were added at pH 7.40. To prepare the ligands, we generated the 3D structure of AP by using ChemBioOffice 2010 and optimized the structure with DS version 3.1. The CDOCKER docking program implemented in DS 3.1 was used for docking simulation in this study.

## 3. Results and discussion

### 3.1. Single-crystal X-ray diffraction

AP crystallization at room temperature was successfully performed with methanol as a solvent. The X-ray diffraction data of AP were collected on an Xcalibur Eos diffractometer. The crystal was kept at 293.15 K during data collection, and the structure of the molecule was identified by Olex2<sup>26</sup> and refined with the ShelXL refinement package by least-squares minimization.<sup>27, 28</sup> Olex2 is a structure solution program that uses charge flipping.<sup>26</sup> The structure of AP was drawn with ORTEP-3. AP crystallizes in a monoclinic system of space group P21/n (14). Additional

crystallographic data are summarized in Table 1, and the corresponding structures are shown in Fig. 1. AP is polymorphic<sup>18–21</sup>; its detected form in the present study could be classified as Form N-1. The AP crystallographic data were deposited at the Cambridge Crystallographic Data Center (CCDC) with supplementary publication number CCDC-1060528. Copies of the data can be obtained free of charge through CCDC at 12 Union Road, Cambridge CB2 1EZ, United Kingdom (e-mail: deposit@ccdc.cam.ac.uk).

The unit cell contains four crystallographically equivalent AP molecules. These molecules are also related to each other by a two-fold screw axis along the *b* direction and *n* glide plane. An AP molecule contains two rings. Two 2-piperidone rings with sofa-half-chair-conformations are connected by the mean planes of the phenyl ring, which are respectively twisted by 68.0(2)° (C8–C7–N1–C5) and 51.2(2)° (C8–C7–N1–C5). The anisole ring is attached to the pyrazole ring twisted by 136.34(16)° (C20–C19–N3–N4). The strongest H bond donor in AP is N(5)–H, and the second strongest bond involves the phenyl ring. Three strong acceptors, namely, C5=O1, C13=O2, and C13=O2, compete for these H bond donors. The AP molecules are connected by H-bonding and form a 3D network (Table 2). N(5)–H donates the shortest N–H···O H bond, i.e., N5–H···O1, which has an H–O separation of only 2.123 Å.

### 3.2. Fluorescence quenching measurement

HSA fluorescence originates from the tryptophan (Trp), tyrosine (Tyr), and phenylalanine (Phe) residues, whereas HSA emission is primarily attributed to the Trp-214 residue. The Phe residue has a very low quantum yield; thus, the energy absorbed by Phe and Tyr is often transferred to the Trp residues in the same protein.<sup>29</sup> In the present work, the HSA concentration was kept at 2.0 μM, and the AP concentration varied from 0 μM to 24.0 μM based on preliminary experiments. The fluorescence spectra were obtained in the range of 300–500 nm at 301, 310, and 318 K. The fluorescence spectra of HSA in the presence and absence of AP at 301 K under excitation at 280 nm is shown in Fig. 2. HSA exhibits a strong fluorescence emission peak at 338 nm, and the intensity of this peak decreases with addition of AP when the HSA concentration is fixed at 2.0 μM. Whereas only tryptophanyl residues are excited at 295 nm, excitation at 280 nm also excited tyrosyl groups.<sup>29, 30</sup> The gap between the quenching curve of  $\lambda_{\text{ex}} = 280$  nm and  $\lambda_{\text{ex}} = 295$  nm gradually increased with increasing AP concentration at 301 K (Fig. 3a). Consequently, both types of fluorophores may participate in AP–HSA interactions. Similar to HSA, AP exhibited quenching and fluorescence emission at 464 nm. The fluorescence intensity of AP when HSA is present (solid line) in the reaction system obviously decreased compared with that of pure AP (dashed line). By selecting the maximum intensities of the AP–HSA and pure-AP systems as references, a relatively linear relationship between the fluorescence intensity and concentration of AP was found (Fig. 3b). Fluorescence intensity decreased by approximately 20% at the corresponding concentrations studied throughout the entire reaction. This finding suggests that AP is also quenched to a certain extent and that interaction occurs between AP and HSA.

Fluorescence quenching refers to any process that decreases the fluorescence

intensity of a sample. A variety of molecular interactions can decrease the fluorescence. These interactions include excited-state reactions, molecular rearrangements, energy transfer, ground-state complex formation, and collisional quenching.<sup>29</sup> Resonance energy transfer (RET) is a type of interaction that can decrease the intensity of the donor and result in energy transfer to an acceptor. This phenomenon only occurs when the absorption spectrum of an acceptor molecule overlaps the fluorescence emission spectrum of a donor molecule. The HSA and AP concentrations were kept at 10.0  $\mu\text{M}$ , and the fluorescence spectra of HSA was measured with 5/5 nm (excitation/emission) slit widths. The emission spectrum of the HSA showed little overlap with the absorption spectrum of AP (Fig. S2). RET is well-known to produce excited acceptors.<sup>29</sup> However, the fluorescence of AP was quenched by approximately 20% in the present study. Therefore, the possibility of energy transfer from HSA to AP is low. Even when RET occurs, only a minimal amount of energy is transferred from HSA to AP.

The primary concern of this study is the collisional or dynamic quenching resulting from collisions between HSA and AP. The well-known Stern–Volmer equation can be used to validate the quenching mechanism by analyzing the fluorescence data at different temperatures:<sup>31, 32</sup>

$$F_0/F = K_{SV}[Q] + 1 \quad (2)$$

where  $F_0$  and  $F$  are the fluorescence intensities in the absence and presence of the quencher, respectively, and  $K_{SV}$  is the Stern–Volmer quenching constant (represented by  $K_D$  if quenching is dynamic). The calculated  $K_{SV}$  (Fig. S3a) values at 301, 310, and 318 K are summarized in Table 3. Dynamic and static quenching are caused by diffusion and ground-state complex formation, respectively; both phenomena can be distinguished by their varying temperature dependence. Dynamic quenching constants are expected to increase with temperature because they are diffusion-dependent.<sup>33, 34</sup> By contrast, complex stability decreases at high temperatures, thereby producing a low static quenching constant.  $K_{SV}$  gradually decreased with increasing temperature in the present study. Thus, the observed quenching follows a static mechanism and is dependent on complex formation.

The use of fluorescence lifetime measurements can help distinguish static quenching from dynamic quenching.<sup>35, 36</sup> The formation of static ground-state complexes does not decrease the decay time of the uncomplexed fluorophores.<sup>35</sup> Dynamic quenching is a rate process that acts on the entire excited-state population and consequently decreases the mean decay time of the entire excited-state population. Time-resolved fluorescence lifetime measurements were conducted to substantiate the static quenching mechanism between HSA and AP. The time-resolved HSA fluorescence quenching by AP was recorded at 280 nm as the excitation wavelength and 338 nm as the emission wavelength. The HSA concentration was fixed at 2.0  $\mu\text{M}$ , whereas the AP concentration was varied from 4  $\mu\text{M}$  to 12  $\mu\text{M}$  at room temperature. The data obtained were analyzed by the tail-fitting method, and the quality of each fit was assessed by  $\chi^2$  values and residuals. The mean fluorescence lifetimes ( $\langle\tau\rangle$ ) for biexponential iterative fitting were calculated from the decay times and pre-exponential factors ( $\alpha$ ) by using the following equation:

$$\langle \tau \rangle = \alpha_1 \tau_1 + \alpha_2 \tau_2. \quad (3)$$

We chose the mean fluorescence lifetime as an important parameter to explore the behavior of HSA molecules bound to AP. Data show that the average lifetime of the HSA fluorophore marginally decreased from 5.337 ns to 5.199 ns with increasing AP concentration (Table 4). The bound AP may directly influence the fluorophore lifetime, and the observed fluorescence originated from the uncomplexed fluorophores. A minimal decrease in the average lifetime of uncomplexed fluorophores was noted with increasing AP concentration (Fig. 4 and Table 4). This alteration of the average fluorescence lifetime in the tested systems suggests the formation of a complex between AP and HSA. Fluorescence quenching is a static mechanism because of ground-state complex formation, which is consistent with the fluorescence quenching analysis results. Therefore, complex formation is the primary factor influencing the AP-induced reduction of HSA fluorescence intensity.

### 3.3 Identification of HSA main binding site

#### 3.3.1 Effect of probes on AP–HSA binding

The HSA monomer contains 585 amino acid residues in three homologous  $\alpha$ -helical domains (I–III). Each domain contains 10 helices and is divided into antiparallel 6-helix and 4-helix subdomains (A and B, respectively).<sup>38, 39</sup> Crystallographic analysis showed that HSA contains multiple binding sites to which various ligands can bind. Two primary sites, 1 and 2,<sup>25</sup> in subdomains IIA and IIIA, respectively, are highly adaptable for binding to several commonly used drugs (e.g., WF and IB). The residues of sites 1 and 2 on the protein are key determinants of binding specificity, as both pockets accommodate binding flexibly. Other binding sites were regarded as secondary sites. Previous studies show that WF and PB can specifically bind to site 1. Site 2 displays affinity to IB, flufenamic acid, and other drugs. Although few ligands have been found to bind to one or several secondary binding sites, most substances bind to sites 1 or 2 or to both sites. Thus, most of the previous work on drug–serum albumin interactions focuses on sites 1 and 2 to locate the main binding sites (the number of secondary drug binding sites on the protein is unknown).<sup>40–42</sup>

WF and IB are frequently used as probes.<sup>43</sup> However, the fluorescence emission of the WF solution decreased (Fig. 5) when AP was present at a concentration of 10.0  $\mu\text{M}$  and the WF concentration was varied from 0  $\mu\text{M}$  to 25.0  $\mu\text{M}$  ( $\lambda_{\text{ex}} = 280 \text{ nm}$ ). By contrast, the fluorescence emission of the AP solution increased but did not show the simple superposition of the WF and AP spectra. On the one hand, AP is excited to a certain extent, which indicates that the AP–WF interaction exists. On the other hand, PB and IB hardly change the fluorescence emission of AP. Consequently, displacement experiments were performed in the current study with PB and IB as site probes to establish the main AP-binding sites of HSA. The HSA and AP concentrations were kept at 2.0  $\mu\text{M}$ , and varying concentrations (0–12.0  $\mu\text{M}$ ) of PB and IB were added to the binary complex. Based on the method of Sudlow et al.,<sup>23</sup> the following equation was used to determine the percentage ( $I_{\text{per}}$ ) of probe displacement:

$$I_{\text{per}} = F/F_0 \quad (4)$$

where  $F$  and  $F_0$  represent the fluorescence intensities of AP–HSA in the absence and

presence of the probe, respectively. Increasing the PB concentration significantly decreased the AP–HSA complex fluorescence intensity (Fig. 6). The original balance was disturbed when PB was added to the binary complex. PB competed with AP because these two drugs share the same binding sites. By contrast, fluorescence intensity was not significantly changed in the case of IB because this molecule exerts limited influence on the binary complex. These results suggest that AP is mainly bound to site 1 of HSA.

### 3.3.2 Molecular docking of the AP–HSA interaction

Molecular docking has been widely employed as a complementary application to improve the current understanding of HSA–drug interactions.<sup>44</sup> This strategy has been applied in receptor-based structural screening techniques to determine active compounds by filtering those that do not fit in the binding sites. CDOCKER is a molecular dynamic simulated-annealing-based algorithm that allows estimation of binding sites.<sup>45–47</sup> It is a grid-based molecular docking method that employs CHARMM.<sup>48–50</sup> The name CDOCKER originates from metallurgical annealing, which involves the heating and controlled cooling of a material to increase crystal orders and reduce defects.<sup>51</sup> Molecular docking is performed by simulated annealing to minimize the CDOCKER energy ( $E_{CD}$ , kcal/mol) and obtain the optimum position. By using a binding site sphere, specifying the ligand placement in the active site is possible.

PB and IB were chosen as probes in Section 3.3.1 of this study, and 2BXC/2BXG was defined as the total receptor by exclusively selecting the protein part for the “Define Receptor” function. In 2BXC, PB was clustered at the center of the site 1 pocket. In 2BXG, IB was clustered at the center of the binding pocket of site 2 and oriented with at least one O atom in the polar patch vicinity. However, IB also occupied a secondary site at the interface between subdomains IIA and IIB in 2BXG. The second site was not considered further because this work only focused on sites 1 and 2 as the main binding sites. By selecting only PB/IB with a “Radius” of 2.5 Å, amino acids within a 2.5 Å radius were chosen, and the site sphere was built with the “From Current Selection” function. Thus, the pre-existing PB/IB was removed. Freshly prepared AP was added, and CHARMM was selected as the force field. The heating procedure was set at 2000 K, and the target heating temperature was 700 K. Heat causes the atoms to leave their initial positions with the local minimum internal energy and move randomly through states of higher energy. The cooling procedure was set at 5000 K, with a target cooling temperature of 300 K.<sup>52, 53</sup> The slow cooling procedure allows ample time for atom redistribution to achieve configurations with lower internal energies than the initial state. Ten molecular docking poses were saved for each site and ranked according to  $-E_{CD}$ . This score considers both internal ligand strain energies and receptor–ligand interaction energies; thus,  $-E_{CD}$  was used to sort the poses of each input ligand. The pose cluster radius was set at 0.5 Å. Results showed that AP has ten docking poses in site 1 but no docking poses in site 2. AP was mainly clustered in site 1 of HSA.

### 3.3.3 Effect of AP-binding on the esterase-like activity of HSA

HSA is primarily a transport protein with catalytic functions, such as hydrolytic and esterase-like activity. HSA can act as an esterase of *p*-nitrophenyl acetate (*p*-NPA),

and this activity results in the acetylation of a tyrosine residue.<sup>54</sup> The residues Arg-410 and Tyr-411 in subdomain IIIA (site 2) play crucial roles in the esterase-like activity of HSA.<sup>55</sup> Site 1 is not involved in this interaction, and site-1-drugs do not inhibit the reaction at low drug-to-HSA ratio.<sup>56,57</sup> Thus, the catalytic activity of HSA in p-NPA was investigated to ascertain the involvement of Arg-410 and Tyr-411 in AP binding.<sup>58</sup>

The Michaelis–Menten plots of p-NPA hydrolysis at different AP:HSA concentrations (0:1, 1:1, and 2:1) were analyzed to deduce the  $k_{cat}$  and  $K_m$  values. The concentration of HSA was kept constant at 10  $\mu$ M, whereas the concentration of p-NPA was varied from 25  $\mu$ M to 700  $\mu$ M. The rate of p-NPA hydrolysis was determined by measuring the concentration of *p*-nitrophenol (yellow product) at 400 nm. The concentration of *p*-nitrophenol was determined from the observed absorbance and a standard curve ( $y = 0.01274x + 0.00444$ ;  $R = 0.9999$ ). The kinetic parameters ( $k_{cat}$  and  $K_m$ ) were determined according to the Michaelis–Menten method<sup>59</sup> (Fig. S4) by fitting the data to the following equations:

$$v = \frac{V_{max}[S]}{K_m + [S]} \quad (5)$$

$$k_{cat} = \frac{V_{max}}{[E]} \quad (6)$$

where  $v$  and  $V_{max}$  are the initial and maximum velocities of hydrolysis, respectively,  $[S]$  is the substrate concentration used,  $[E]$  is the enzyme concentration, and  $k_{cat}$  and  $K_m$  are kinetic parameters. AP did not inhibit p-NPA hydrolysis by HSA at the test mole ratios investigated (Table 5 and Fig. 7). Therefore, Arg-410 and Tyr-411 in site 2 are not unaffected by AP. These results suggest that AP almost never binds to site 2 but is highly likely to bind to site 1. Therefore, AP binding to site 1 was confirmed.

### 3.4 Binding mode

AP-induced HSA fluorescence quenching is a static process; thus, the binding constant ( $K$ ) and the number of complexes bound to HSA ( $n$ ) were determined by plotting the double-logarithm regression curve of the fluorescence data according to the following “modified” Stern–Volmer equation:

$$\log(F_0 - F)/F = \log K + n \log [Q] \quad (7)$$

where  $K$  is the binding constant of the site, and  $n$  is the binding site multiplicity per class of binding site. The results are summarized in Table 6. The values of  $K$  (Fig. S3b) suggest a strong binding force between AP and HSA. The value of  $n$  (approximately equal to 1) suggests the presence of a single high-affinity binding site in HSA.

The thermodynamic parameters of the binding reaction confirm the presence of intermolecular forces. Changes in the enthalpy ( $\Delta H^0$ ) and entropy ( $\Delta S^0$ ) can help confirm the binding modes.  $\Delta H^0$  and  $\Delta S^0$  can be calculated by the van't Hoff equation as:<sup>60</sup>

$$\ln K = -\frac{\Delta H^0}{RT} + \frac{\Delta S^0}{R} \quad (8)$$

where  $K$  is analogous to the associative binding constant at the corresponding temperature, and  $R$  is the gas constant. The free-energy change ( $\Delta G^0$ ) can be estimated as:

$$\Delta G^0 = \Delta H^0 - T\Delta S^0 = -RT \ln K \quad (9)$$

The results are presented in Table 6. The negative  $\Delta G^0$  values indicate that the binding of AP with HSA spontaneously occurs. Four representative interaction forces, namely, hydrophobic forces, H bonds, van der Waals (VDW) forces, and electrostatic interactions, generally exist between small molecular substrates and biological macromolecules. According to the theory of Ross and Subramanian, negative  $\Delta H^0$  and  $\Delta S^0$  values indicate H-bonding; VDW forces play major roles in AP–HSA binding.

AP mainly binds to site 1; thus, the position with the highest  $-E_{CD}$  in site 1 was chosen to be the most suitable for the analysis. AP was well inserted into the hydrophobic cavity of the active site (site 1; Fig. 8). In addition, AP was well attached between the polar side-chains of Leu-238 and Ala-291 (Panel 3D). This trend is particularly evident at the mouth of the pocket, where a wide opening that provides significant room for movement may be observed.<sup>25</sup> AP was closely bound to Trp-214 and inevitably quenched its fluorescence, as determined from the combined results of Section 3.2. Gaps in the active site of the AP–HSA complex were not favored. When AP is inserted into HSA, both molecules undergo changes under the influence of VDW forces to minimize the space between them.<sup>61</sup> VDW forces have been used as a general term to refer to a variety of nonspecific interactions, such as dipole–dipole, multipole–multipole, induced dipole–induced dipole, and even cation–dipole interactions; recent studies have gradually revealed the details behind these distinguishable interactions.<sup>62</sup> Interactions involving  $\pi$  electron systems have specifically been shown to include cations and CH groups, and  $\pi$ –cation interactions occur between a positively charged molecule and a  $\pi$  system. Panel 2D shows the  $\pi$ –cation interactions at pH 7.40. Lys-195, Lys-199, and Arg-218 act as cations that participate in these intermolecular interactions. Intramolecular  $\pi$ –cation interactions also occur between the two phenyl rings. AP easily forms hydrogen bonds because of its strong donor and acceptor groups (Section 3.1). The Arg-218 residue of HSA forms an intermolecular H bond with O(2) (2.216 Å), whereas Arg-222 forms two H bonds with O(1) (2.330 Å) and O(2) (2.243 Å). H-bonding during AP–HSA complex formation can effectively balance the adverse energetic effects of water displacement.

### 3.5 Effect of AP on the HSA conformation

#### 3.5.1. 3D fluorescence spectroscopy

3D fluorescence spectroscopy can provide detailed information on the conformational and microenvironmental changes of proteins combining with small molecules.<sup>58</sup> The 3D fluorescence spectra of HSA (2.0  $\mu$ M) and the AP–HSA complex (molar ratio, 4:1) were obtained at an excitation wavelength range of 200–400 nm at increments of 5 nm. The emission spectra were also monitored between 200 and 500 nm. The 3D fluorescence contour maps of HSA and the AP–HSA system are shown in Fig. 9. Peak A is a second-order scattering peak, and its emission wavelength is twice its excitation wavelength ( $\lambda_{em} = 2\lambda_{ex}$ ). Peak B refers to the Rayleigh scattering peak ( $\lambda_{em} = \lambda_{ex}$ ), which is common to all spectra. Peak 3

represents the AP peak, which appears for the first time in Fig. 9b. The peak position, intensity, and Stokes' shift of the fluorescence spectra are summarized in Table 7. After AP addition, the positions of the excitation and emission wavelengths, as well as their Stokes' shift, remained nearly unchanged. The molecular microenvironment around the fluorophore residues of HSA was only minimally affected. Peak 1 mainly exhibited the fluorescence characteristics of polypeptide backbone structures. The fluorescence intensity of peak 1 decreased after AP addition, which indicates changes in the peptide strand structure of HSA. Peak 2 mainly revealed the spectral behavior of Trp and Tyr residues. The decreased fluorescence intensity of peak 2 indicates that AP affects Trp, Tyr, or both residues. This result agrees with the results in Section 3.2.

### 3.5.2. CD spectroscopy

CD is a universally-acknowledged technique commonly used to characterize the structure of proteins.<sup>63</sup> To investigate the effect of AP binding on the conformational changes in HSA, CD spectroscopic analysis was performed on free HSA and the AP-HSA complex. CD was measured with a constant HSA concentration of 2.0  $\mu\text{M}$ , but the complex concentrations were varied from 0  $\mu\text{M}$  to 16.0  $\mu\text{M}$  [ $r_i = (\text{AP})/(\text{HSA}) = 0:1, 2:1, 8:1$ ]. Each spectrum was scanned thrice and averaged for graphing and analyses. HSA exhibits two negative ellipticities at 208 and 220 nm (Fig. 10), which are characteristic of  $\alpha$ -helix structures in proteins. The shapes of the CD spectra with and without AP were similar, which suggests that the HSA structure is also predominantly an  $\alpha$ -helix. The negative bands did not shift, and their intensity remained nearly constant if system errors are taken into consideration. CD data were then analyzed using the SELCON3 method to quantify the different contents of the secondary structures of HSA.<sup>64</sup> Table 8 lists the percentage composition of  $\alpha$ -helix (the total content of regular and distorted  $\alpha$ -helix),  $\beta$ -sheet,  $\beta$ -turn and random coils in free HSA, AP-HSA systems. AP presents minimal effects on the secondary structure of HSA. As a transport protein, HSA displays nonspecific and reversible drug interactions. H-bonding is indispensable in the formation of the secondary and tertiary structures of HSA. The 3D structures and functions of several biological molecules are highly dependent on intramolecular H-bonding. Newly-formed H bonds do not show significant effects on the original bonding, and this minimal change may be beneficial for HSA.

## 4. Conclusions

This paper reports the single crystallographic data of AP obtained with methanol as a solvent. AP crystallizes as a monoclinic system of the P21/n (14) space group, and its current form was classified as Form N-1. Experimental data showed that AP could be inserted into HSA and quench intrinsic HSA fluorescence via a static mechanism induced by the formation of an AP-HSA complex. Tyrosine and tryptophan participated in the AP-HSA interaction. AP fluorescence also decreased by approximately 20%. The possibility of energy transfer from HSA to AP was low. Even with energy transfer, only a minimal amount of energy is transferred from HSA to AP. Studies on the fluorescence and fluorescence lifetime confirmed that quenching occurs via a static mechanism. Complex formation was the primary factor influencing the AP-induced decrease in HSA fluorescence intensity. AP could also interact with

WF. Displacement and molecular docking experiments demonstrated that the AP binding site is mainly located in site 1 of HSA. The effects of AP binding on the esterase-like activity of HSA study confirmed this binding site. AP contains strong donor and acceptor groups that easily form intramolecular and intermolecular H bonds. H-bonding also played an important role in stabilizing the AP–HSA complex. VDW forces, including  $\pi$ -cation interaction, contributed to the good fit of AP in site 1 of HSA. AP was closely bound to Trp-214 and snugly pinned between the apolar side-chains of Leu-238 and Ala-291, thereby allowing room for significant movement. Conformation studies showed that AP does not significantly affect the local conformation of HSA. This study provides novel insights into the characteristics of AP–HSA binding for the improved utilization of AP during standard screening in pharmaceutical firms and clinical research.

#### Acknowledgements

This work was supported by the Applied Basic Research Project of Sichuan Province (Grant No. 2014JY0042), the Testing Platform Construction of Technology Achievement Transform of Sichuan Province (Grant No. 13CGPT0049), and the National Development and Reform Commission and Education of China (Grant No. 2014BW011).

#### References

1. J. Heit, *J. Thromb. Haemost.*, 2005, **3**, 1611-1617.
2. E. Previtali, P. Bucciarelli, S. M. Passamonti and I. Martinelli, *Blood Transfus-Italy*, 2011, **9**, 120.
3. D. Jimenez, R. D. Yusen and E. Ramacciotti, *Adv. Ther.*, 2012, **29**, 187-201.
4. E. D. Deeks, *Drugs*, 2012, **72**, 1271-1291.
5. J. Watson, G. Whiteside and C. Perry, *Drugs*, 2011, **71**, 2079-2089.
6. G. Agnelli, H. R. Buller, A. Cohen, M. Curto, A. S. Gallus, M. Johnson, A. Porcari, G. E. Raskob, J. I. Weitz and P.-E. Investigators, *New Engl. J. Med.*, 2013, **368**, 699-708.
7. C. Roser-Jones and R. C. Becker, *J. Thromb. Thrombolys.*, 2010, **29**, 141-146.
8. C. Frost, J. Wang, S. Nepal, A. Schuster, Y. C. Barrett, R. Mosqueda-Garcia, R. A. Reeves and F. LaCreta, *Brit. J. Clin. Pharmacol.*, 2013, **75**, 476-487.
9. C. H. Yeh, K. Hogg and J. I. Weitz, *Arterioscl. Throm. Vas.*, 2015, **35**, 1056-1065.
10. P. C. Wong, D. J. Pinto and D. Zhang, *J. Thromb. Thrombolys.*, 2011, **31**, 478-492.
11. A. S. Committee, Investigators, J. H. Alexander, R. C. Becker, D. L. Bhatt, F. Cools, F. Crea, M. Dellborg, K. A. Fox, S. G. Goodman, R. A. Harrington, K. Huber, S. Husted, B. S. Lewis, J. Lopez-Sendon, P. Mohan, G. Montalescot, M. Ruda, W. Ruzyllo, F. Verheugt and L. Wallentin, *Circulation*, 2009, **119**, 2877-2885.
12. C. Frost, Z. Yu, K. Moore, S. Nepal, Y. Barrett, R. Mosqueda-Garcia and A. Shenker, *J. Thromb. Haemost.*, 2007, **5**, abstract PM-664.
13. Z.-m. Wang, J. X. Ho, J. R. Ruble, J. Rose, F. Rüker, M. Ellenburg, R. Murphy, J. Click, E. Soistman, L. Wilkerson and D. C. Carter, *BBA - Subjects*, 2013,

- 1830**, 5356-5374.
14. P. A. Zunszain, J. Ghuman, A. F. McDonagh and S. Curry, *J. Mol. Biol.*, 2008, **381**, 394-406.
  15. P. A. Alexander, Y. He, Y. Chen, J. Orban and P. N. Bryan, *Proc. Natl. Acad. Sci. U.S.A.*, 2009, **106**, 21149-21154.
  16. Z. Chen, H. Xu, Y. Zhu, J. Liu, K. Wang, P. Wang, S. Shang, X. Yi, Z. Wang, W. Shao and S. Zhang, *RSC Adv.*, 2014, **4**, 25410.
  17. A. S. Sharma, S. Anandakumar and M. Ilanchelian, *RSC Adv.*, 2014, **4**, 36267-36281.
  18. *US Pat.*, 7 396 932, 2005.
  19. *US Pat.*, 0 203 178, 2007.
  20. *US Pat.*, 0 245 267, 2013.
  21. *US Pat.*, 0 018 386, 2015.
  22. G. Sudlow, D. Birkett and D. Wade, *Mol. Pharmacol.*, 1975, **11**, 824-832.
  23. G. Sudlow, D. Birkett and D. Wade, *Mol. Pharmacol.*, 1976, **12**, 1052-1061.
  24. M. Shahlaei, B. Rahimi, M. R. Ashrafi-Kooshk, K. Sadrjavadi and R. Khodarahmi, *J. Lumin.*, 2015, **158**, 91-98.
  25. J. Ghuman, P. A. Zunszain, I. Petitpas, A. A. Bhattacharya, M. Otagiri and S. Curry, *J. Mol. Biol.*, 2005, **353**, 38-52.
  26. O. V. Dolomanov, L. J. Bourhis, R. J. Gildea, J. A. K. Howard and H. Puschmann, *J. Appl. Crystallogr.*, 2009, **42**, 339-341.
  27. G. M. Sheldrick, *Acta Crystallogr., Sect. A: Found. Crystallogr.*, 2008, **64**, 112-122.
  28. C. B. Hubschle, G. M. Sheldrick and B. Dittrich, *J. Appl. Crystallogr.*, 2011, **44**, 1281-1284.
  29. J. R. Lakowicz, *Principles of fluorescence spectroscopy*, Springer, Singapore, 3rd edn., 2009.
  30. J. Równicka-Zubik, L. Sułkowski, M. Maciążek-Jurczyk and A. Sułkowska, *J. Mol. Struct.*, 2013, **1044**, 152-159.
  31. X. Zhao, R. Liu, Z. Chi, Y. Teng and P. Qin, *J. Phys. Chem. B*, 2010, **114**, 5625-5631.
  32. X. Zhao, R. Liu, Y. Teng and X. Liu, *Sci. Total Environ.*, 2011, **409**, 892-897.
  33. X. Zhao, F. Sheng, J. Zheng and R. Liu, *J. Agr. Food Chem.*, 2011, **59**, 7902-7909.
  34. X. Zhao, D. Lu, F. Hao and R. Liu, *J. Hazard. Mater.*, 2015, **292**, 98-107.
  35. L. A. MacManus-Spencer, M. L. Tse, P. C. Hebert, H. N. Bischel and R. G. Luthy, *Anal. Chem.*, 2009, **82**, 974-981.
  36. P. C. Hebert and L. A. MacManus-Spencer, *Anal. Chem.*, 2010, **82**, 6463-6471.
  37. Q. Wang, J. He, X. Ma, Y. Li and H. Li, *RSC Adv.*, 2015, **5**, 44696-44704.
  38. A. J. Ryan, J. Ghuman, P. A. Zunszain, C. W. Chung and S. Curry, *J. Struct. Biol.*, 2011, **174**, 84-91.
  39. I. Petitpas, T. Grüne, A. A. Bhattacharya and S. Curry, *J. Struct. Biol.*, 2001, **314**, 955-960.

40. O. A. Hamdi, S. R. Feroz, J. A. Shilpi, H. Anouar el, A. K. Mukarram, S. B. Mohamad, S. Tayyab and K. Awang, *Int. J. Mol. Sci.*, 2015, **16**, 5180-5193.
41. J. Wei, F. Jin, Q. Wu, Y. Jiang, D. Gao and H. Liu, *Talanta*, 2014, **126**, 116-121.
42. X. Xu, Y. Qian, P. Wu, H. Zhang and C. Cai, *J. Colloid Interf. Sci.*, 2015, **445**, 102-111.
43. Q. Wang, J. He, D. Wu, J. Wang, J. Yan and H. Li, *J. Lumin.*, 2015, **164**, 81-85.
44. S. R. M and F.-M. Janet, *Computational and Structural Approaches to Drug Discovery : Ligand-Protein Interactions*, Royal Society of Chemistry, UK, 2008.
45. M. Vieth, J. D. Hirst, B. N. Dominy, H. Daigler and C. L. Brooks, *J. Comput. Chem.*, 1998, **19**, 1623-1631.
46. M. Vieth, J. D. Hirst, A. Kolinski and C. L. Brooks, *J. Comput. Chem.*, 1998, **19**, 1612-1622.
47. G. Wu, D. H. Robertson, C. L. Brooks and M. Vieth, *J. Comput. Chem.*, 2003, **24**, 1549-1562.
48. A. J. Maynard, T. Ehlers and J. Koska, Abstracts of Papers, 240th ACS National Meeting, Boston, MA, United States, August, 2010.
49. D. Abuo-Rahma Gel, M. Abdel-Aziz, N. A. Farag and T. S. Kaoud, *Eur. J. Med.Chem.*, 2014, **83**, 398-408.
50. J. Bie, S. Liu, J. Zhou, B. Xu and Z. Shen, *Bioorg. Med. Chem*, 2014, **22**, 1850-1862.
51. Y. Dai, N. Chen, S. Jia, Q. Wang, Dong, Lilong, Zheng, Heng, Zhang, Xiuli and D. Feng, *Iran. J. Pharm. Res.*, 2012, **11**, 807-830.
52. Q. Wang, Q. Sun, X. Ma, Z. Rao and H. Li, *J. Photochem. Photobiol. B: Biol.*, 2015, **148**, 268-276.
53. *CATALYST version 4.11, Users' Manual, Accelrys Software Inc., San Diego, 2005.*
54. G. E. Means and M. L. Bender, *Biochemistry*, 1975, **14**, 4989-4994.
55. O. Yoshiro, K. Yukihiisa, Yotsuyanagi and K. Ikeda, *Chem. Pharm. Bull.*, 1980, **28**, 535-540.
56. A. Awad-Elkarim and G. E. Means, *Comp. Biochem. Phys. B*, 1988, **91**, 267-272.
57. H. Watanabe, S. Tanase, K. Nakajou, T. Maruyama, U. Kragh-Hansen and M. Otagiri, *Biochem. J.*, 2000, **349**, 813-819.
58. M. T. Rehman, H. Shamsi and A. U. Khan, *Mol. Pharm.*, 2014, **11**, 1785-1797.
59. N. Kamtekar, A. Pandey, N. Agrawal, R. R. Pissurlenkar, M. Borana and B. Ahmad, *PloS one*, 2013, **8**, e53499.
60. R. G. Mortimer, *Physical Chemistry*, Elsevier, Canada, 3rd edn., 2008.
61. G. U. Nienhaus, *Protein-Ligand Interactions*, Springer, USA, 2005.
62. R. A. C. A, *Ligand-Macromolecular Interactions in Drug Discovery*, Springer, London, 2010.
63. M. Ishtikhar, S. Khan, G. Badr, A. Osama Mohamed and R. H. Khan, *Mol.*

- Biosyst.*, 2014, **10**, 2954-2964.
64. N. Sreerama and R. W. Woody, *Anal. Biochem.*, 2000, **287**, 252-260.

**Table 1**

Crystal and experimental data of apixaban

Empirical formula	C <sub>25</sub> H <sub>25</sub> N <sub>5</sub> O <sub>4</sub>
Formula weight	460.48
Temperature/K	293.15
Crystal system	monoclinic
Space group	P2 <sub>1</sub> /n
a/Å	10.2208(4)
b/Å	13.8422(6)
c/Å	15.7529(6)
α/°	90
β/°	92.927(3)
γ/°	90
Volume/Å <sup>3</sup>	2225.79(15)
Z	4
ρ <sub>calc</sub> /cm <sup>3</sup>	1.374
μ/mm <sup>-1</sup>	0.098
F(000)	968.0
Crystal size/mm <sup>3</sup>	0.3 × 0.2 × 0.2
Radiation	MoKα (λ = 0.71073)
2θ range for data collection/°	5.956 to 52.74
Index ranges	-12 ≤ h ≤ 12, -17 ≤ k ≤ 16, -19 ≤ l ≤ 9
Reflections collected	10241
Independent reflections	4539 [R <sub>int</sub> = 0.0197, R <sub>sigma</sub> = 0.0354]
Data/restraints/parameters	4539/0/316
Goodness-of-fit on F <sup>2</sup>	1.028
Final R indexes [I >= 2σ (I)]	R <sub>1</sub> = 0.0460, wR <sub>2</sub> = 0.1048
Final R indexes [all data]	R <sub>1</sub> = 0.0677, wR <sub>2</sub> = 0.1164
Largest diff. peak/hole / e Å <sup>-3</sup>	0.28/-0.27

**Table 2**

Hydrogen bonds for apixaban (Å and °).

D-H...A	d(D-H)	d(H...A)	d(D...A)	<DHA
C9-H9...O1 <sup>a</sup>	0.930	2.604	3.386	142.12
C20-H20...O1 <sup>a</sup>	0.930	2.490	3.403	167.27
C11-H11...O2 <sup>b</sup>	0.930	2.629	3.342	133.95
C21-H21...O3 <sup>c</sup>	0.930	2.393	3.246	152.44
C25-H25C...O3 <sup>d</sup>	0.960	2.619	3.350	133.22
N5-H5A...O1 <sup>d</sup>	0.872	2.123	2.982	168.66

Symmetry codes: <sup>a</sup> -x+2, -y+1, -z, <sup>b</sup> -x+1, -y+1, -z, <sup>c</sup> x+1/2, -y+3/2, z-1/2, <sup>d</sup> -x+3/2, y+1/2, -z+1/2,**Table 3**

Stern-Volmer quenching constants for AP-HSA interaction

T/K	$K_{SV} \times 10^4 (M^{-1})$	R <sup>a</sup>
301	2.544 ± 0.058	0.9990
310	2.340 ± 0.043	0.9993
318	2.174 ± 0.065	0.9982

<sup>a</sup> the correlation coefficient for the  $K_{sv}$  values.**Table 4.** Lifetime of HSA fluorescence decay in Tris-HCl of pH 7.4 at different AP concentrations.

System	$C_{(AP)} (\mu M)$	$\tau_1$	$\tau_2$	$\tau_3$	$\alpha_1$	$\alpha_2$	$\alpha_3$	$\langle \tau \rangle$	$\chi^2$
Free HSA	0.0	0.788	3.640	7.130	0.050	0.423	0.527	5.337	1.055
	4.0	0.847	3.866	7.321	0.060	0.483	0.457	5.265	1.036
AP-HSA	8.0	0.806	3.735	7.105	0.060	0.443	0.497	5.234	1.050
	12.0	0.812	3.703	7.072	0.062	0.441	0.497	5.199	1.067

**Table 5.** Steady-State Kinetic Parameters for Esterase-like Activity of HSA

AP:HSA	$K_m (\mu M)$	$k_{cat} (s^{-1}) \times 10^{-3}$	$k_{cat}/K_m (M^{-1} S^{-1})$
0:1	123.1 ± 4.99	8.764 ± 0.704	71.18 ± 2.83
1:1	120.4 ± 4.08	9.234 ± 0.634	76.70 ± 2.67
2:1	118.9 ± 3.16	9.604 ± 0.524	80.79 ± 2.26

**Table 6**

Binding constants K, binding sites n, and thermodynamic parameters for AP-HSA interaction

T/K	$K \times 10^4 (M^{-1})$	n	R <sup>a</sup>	$\Delta G^0$ (kJ·mol <sup>-1</sup> )	$\Delta H^0$ (kJ·mol <sup>-1</sup> )	$\Delta S^0$ (J·mol <sup>-1</sup> )	R <sup>b</sup>
301	3.407 ± 0.142	1.03 ± 0.02	0.9995	-26.12 ± 0.67			
310	2.460 ± 0.096	1.00 ± 0.02	0.9996	-26.06 ± 1.25	-33.36 ± 3.42	-23.90 ± 11.04	0.9948
318	1.665 ± 0.127	0.97 ± 0.03	0.9983	-25.37 ± 0.53			

<sup>a</sup> is the standard deviation for the K values.<sup>b</sup> the correlation coefficient for the van't Hoff.

**Table 7**

3D fluorescence spectral parameters of HSA alone and in the presence of AP

System	Peaks	Peak position [ $\lambda_{ex}/\lambda_{em}$ (nm/nm)]	Stokes [ $\Delta\lambda$ (nm)]	Intensity
HSA	B	225/225→320/320	0	14.789→316.686
	1	225/331	106	591.454
	2	280/338	58	527.974
AP-HSA	B	235/235→320/320	0	12.246→321.799
	1	225/331	106	474.105
	2	280/337	57	386.107

**Table 8.** Contents of different secondary structures of free HSA and AP-HSA systems.

System	Molar ratio	H(r) (%)	H(d) (%)	S(r) (%)	S(d) (%)	Trn (%)	Unrd (%)
Free HSA	N/A	0.340	0.193	0.046	0.045	0.135	0.241
AP-HSA	2:1	0.342	0.196	0.031	0.040	0.141	0.250
	8:1	0.339	0.193	0.045	0.045	0.137	0.241

H(r): regular  $\alpha$ -helix. H(d): distorted  $\alpha$ -helix; S(r): regular  $\beta$ -strand; S(d): distorted  $\beta$ -strand; Trn: turns; Unrd: unordered structure.

### Figure Captions

**Fig. 1.** Molecular structure of AP showing the atom-numbering scheme.

**Fig. 2.** Fluorescence spectra of AP–HSA (solid line) and of pure AP (dashed line) at 301 K.  $C_{(\text{HSA})} = 2 \mu\text{M}$  (A). The AP concentrations were 4 (B), 8 (C), 12 (D), 16 (E), 20 (F), and 24 (G)  $\mu\text{M}$ .

**Fig. 3.** Panel a: The quenching curve of HSA in the presence of AP obtained at excitation wavelengths of 280 and 295 nm and 301 K. Panel b: The relative intensity of AP in presence (●) and absence (▲) of HSA. ★ represents the intensity ratio of AP (HSA present: HSA absent) at the corresponding concentration.

**Fig. 4.** Time-resolved HSA fluorescence decay in the presence of AP: (A)  $C_{(\text{HSA})} = 2.0 \mu\text{M}$ , (B)–(D)  $C_{(\text{AP})} = 4.0, 8.0, \text{ and } 12.0 \mu\text{M}$ .

**Fig. 5.** Fluorescence spectra of WF in the absence (dashed line) and presence (solid line) of AP. The AP concentration was 10  $\mu\text{M}$  (A), and the WF concentrations were 5 (B), 10 (C), 15 (D), 20 (E), and 25 (F)  $\mu\text{M}$ .

**Fig. 6.** Effect of probes on the fluorescence of AP–HSA complexes.  $C_{(\text{AP})} = C_{(\text{HSA})} = 2.0 \mu\text{M}$ . The molar ratios of probes to AP–HSA complexes were 1:1, 2:1, 3:1, 4:1, 5:1, and 6:1.

**Fig. 7.**  $k_{\text{cat}}$  and  $K_{\text{m}}$  values of HSA in the absence and presence of AP.  $C_{(\text{HSA})} = 10 \mu\text{M}$ . AP concentrations of 10 and 20  $\mu\text{M}$  were applied.

**Fig. 8.** Surface around site 1 of AP. The insets in the figures show the 3D and 2D docking modes between AP and HSA. For the 2D mode, only important interacting residues are shown and represented as sticks. The hit compound is shown in pink. Residues involved in hydrogen bonding, charge, and polar interactions are represented by magenta circles. Residues involved in van der Waals interactions are represented by green circles. The solvent-accessible surfaces of atoms are represented by a blue halo around the atom. The diameter of the circle is proportional to the solvent accessible surface. Hydrogen bonding interactions with amino acid side chains are represented by a blue dash with the arrows directed toward the electron donor.

**Fig. 9.** Contour spectra of (a) HSA and (b) HSA-AP system in Tris–HCl buffer of pH 7.40.  $C_{(\text{HSA})} = 2.0 \mu\text{M}$  and  $C_{(\text{AP})} = 8 \mu\text{M}$ .

**Fig. 10.** Circular dichroism (CD) spectra of free HSA (2  $\mu\text{M}$ ) and the HSA complex with AP ( $r_i = [\text{HSA}]/[\text{AP}] = 1:2, 1:8$ ) at pH 7.40.

**Graphical abstract:** Probing apixaban binding to human serum albumin: combining spectroscopic methods and docking investigations.

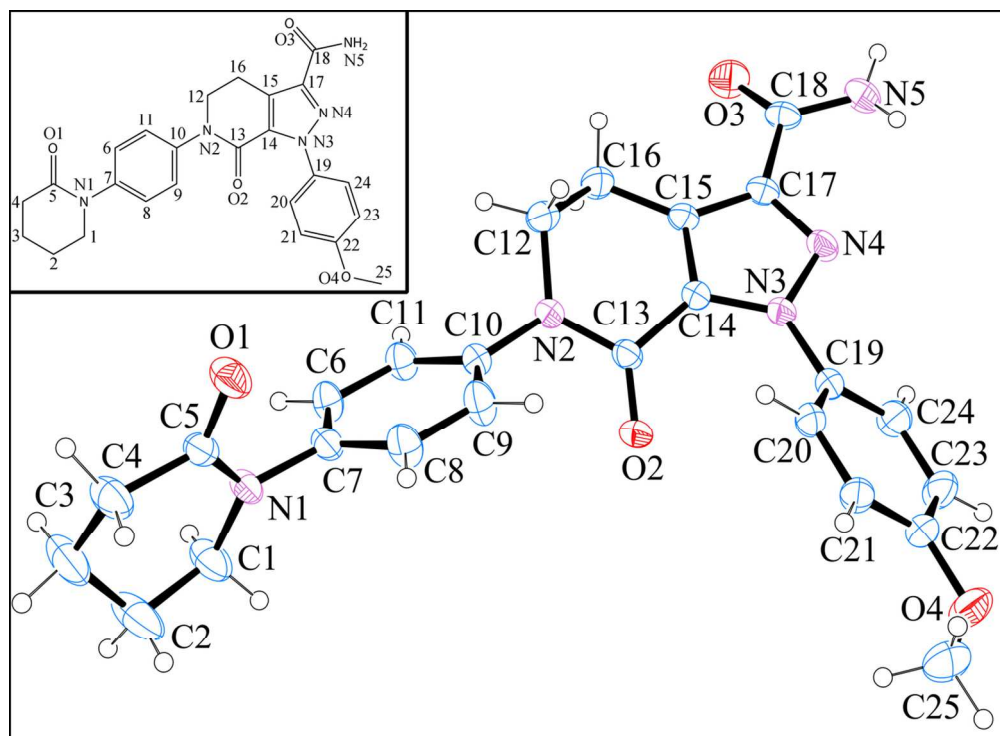


Fig. 1. Molecular structure of AP showing the atom-numbering scheme.  
60x44mm (600 x 600 DPI)

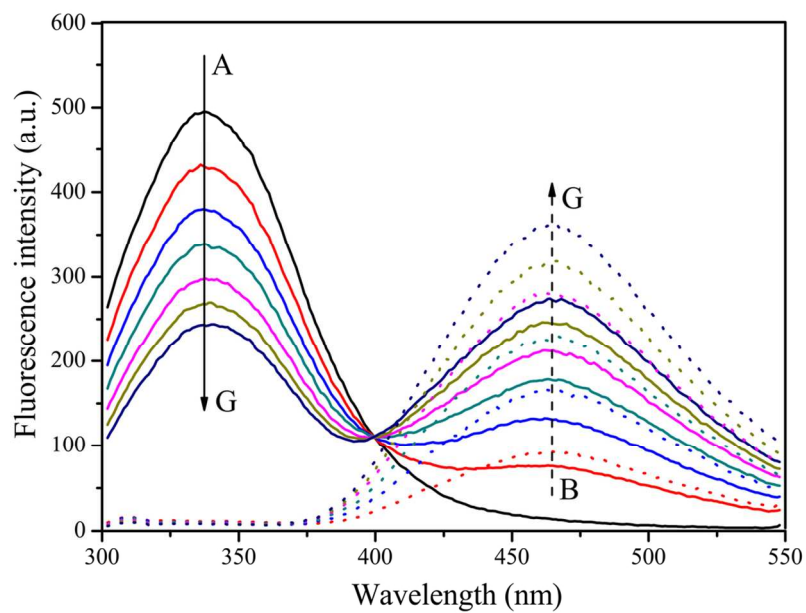


Fig. 2. Fluorescence spectra of AP-HSA (solid line) and of pure AP (dashed line) at 301 K.  $C(\text{HSA}) = 2 \mu\text{M}$  (A). The AP concentrations were 4 (B), 8 (C), 12 (D), 16 (E), 20 (F), and 24 (G)  $\mu\text{M}$ .  
58x41mm (600 x 600 DPI)

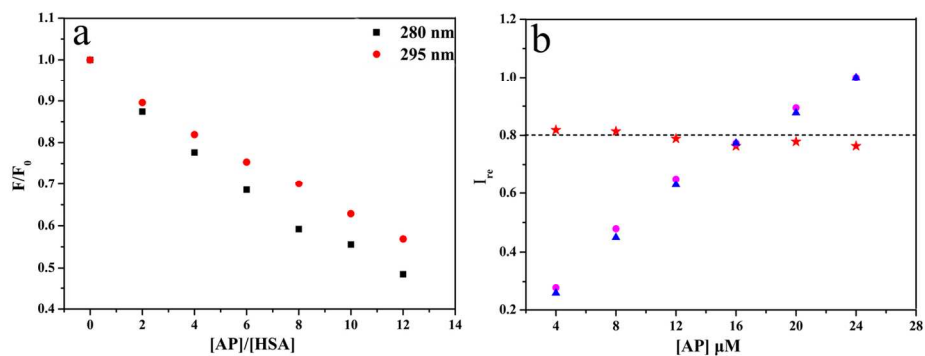


Fig. 3. Panel a: The quenching curve of HSA in the presence of AP obtained at excitation wavelengths of 280 and 295 nm and 301 K. Panel b: The relative intensity of AP in presence (●) and absence (▲) of HSA. ★ represents the intensity ratio of AP (HSA present: HSA absent) at the corresponding concentration. 69x27mm (600 x 600 DPI)

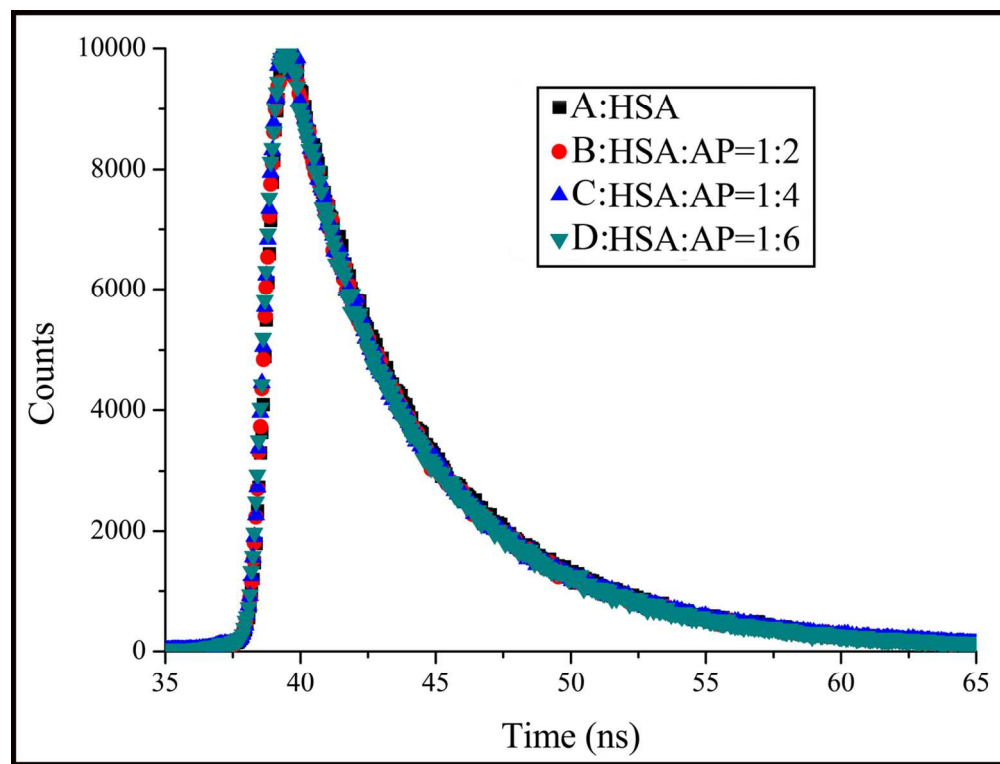


Fig. 4. Time-resolved HSA fluorescence decay in the presence of AP: (A)  $C(\text{HSA}) = 2.0 \mu\text{M}$ , (B)–(D)  $C(\text{AP}) = 4.0, 8.0,$  and  $12.0 \mu\text{M}$ .  
62x47mm (600 x 600 DPI)

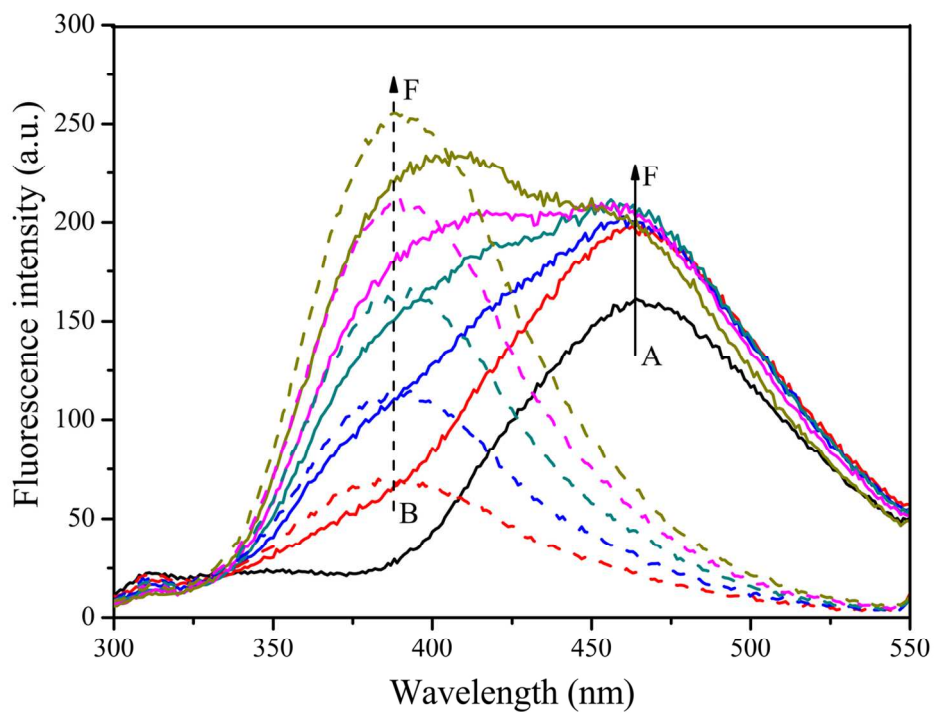


Fig. 5. Fluorescence spectra of WF in the absence (dashed line) and presence (solid line) of AP. The AP concentration was 10  $\mu\text{M}$  (A), and the WF concentrations were 5 (B), 10 (C), 15 (D), 20 (E), and 25 (F)  $\mu\text{M}$ .  
62x47mm (600 x 600 DPI)

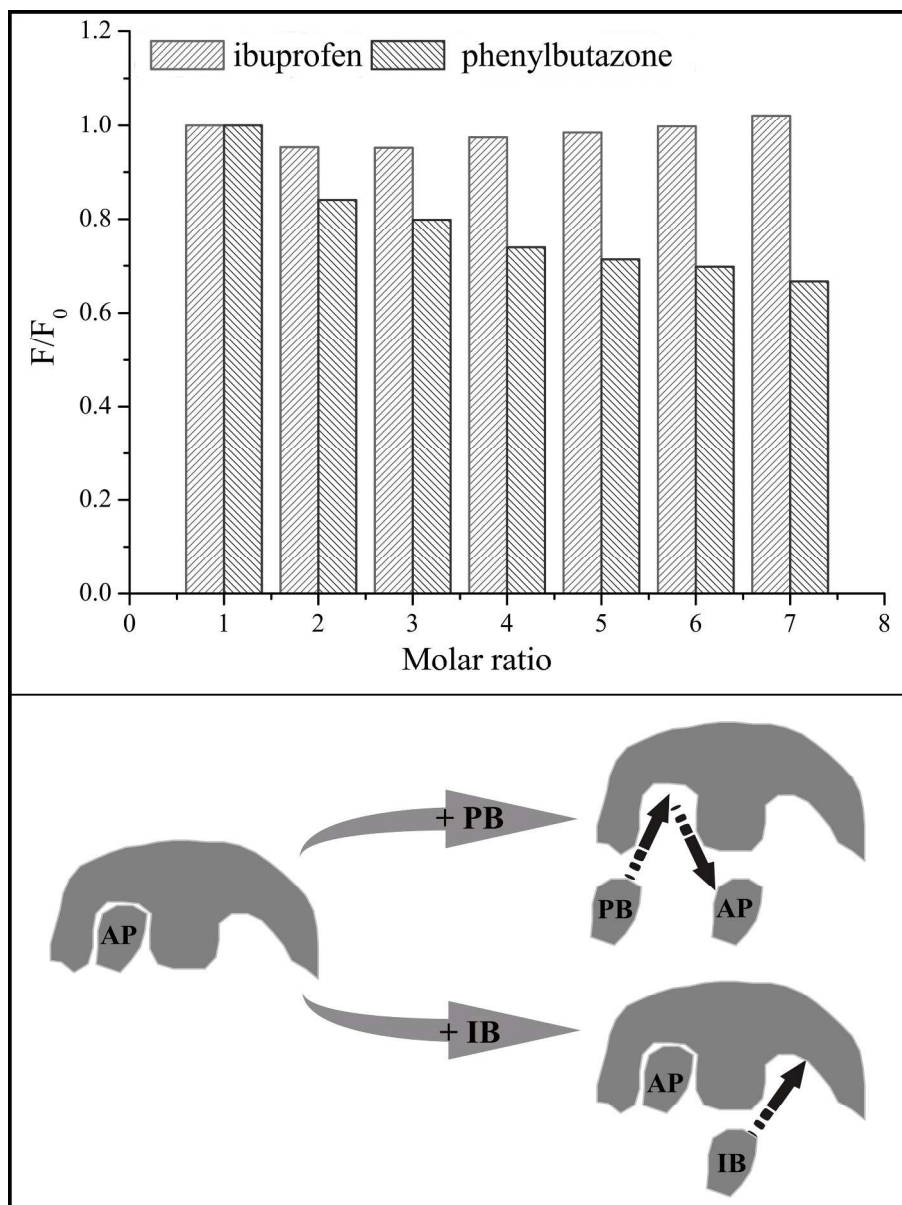


Fig. 6. Effect of probes on the fluorescence of AP-HSA complexes.  $C(\text{AP}) = C(\text{HSA}) = 2.0 \mu\text{M}$ . The molar ratios of probes to AP-HSA complexes were 1:1, 2:1, 3:1, 4:1, 5:1, and 6:1.  
109x145mm (600 x 600 DPI)

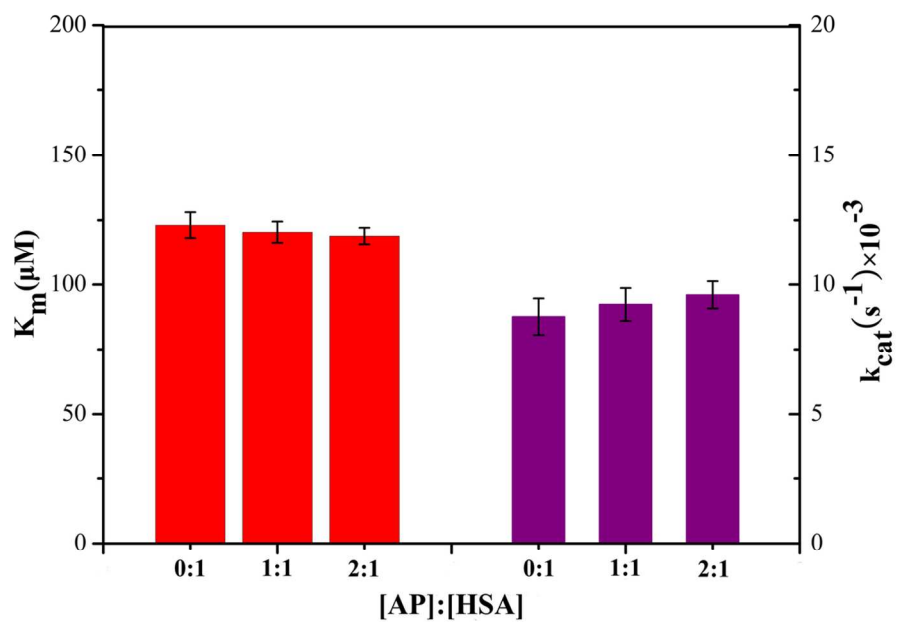


Fig. 7. k<sub>cat</sub> and K<sub>m</sub> values of HSA in the absence and presence of AP. C(HSA) = 10 µM. AP concentrations of 10 and 20 µM were applied.  
57x39mm (600 x 600 DPI)

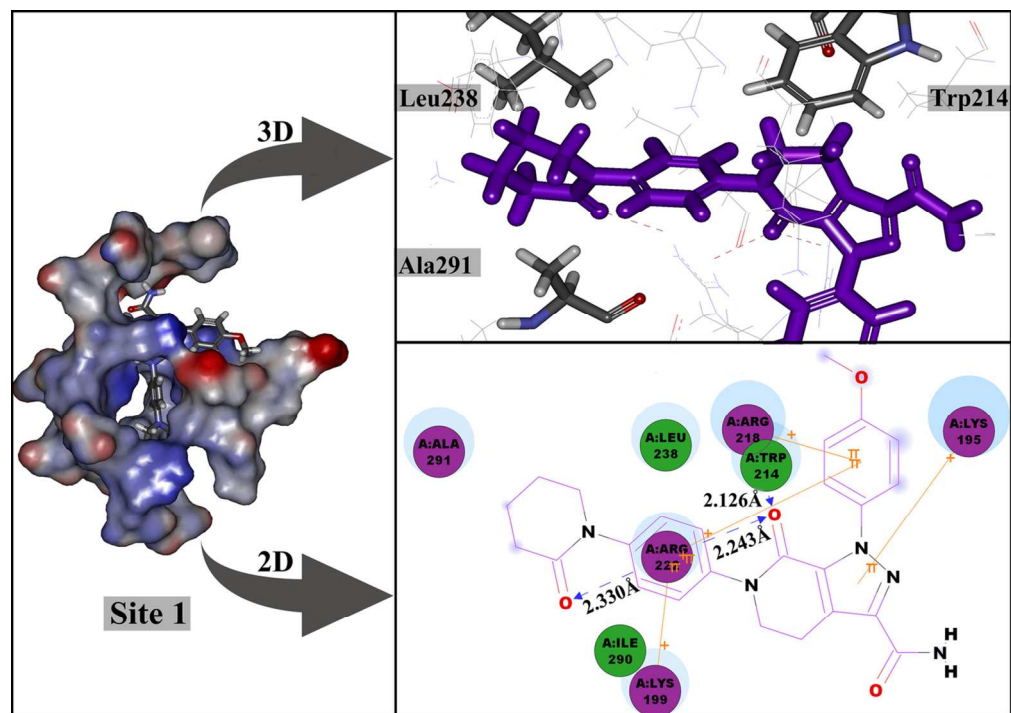


Fig. 8. Surface around site 1 of AP. The insets in the figures show the 3D and 2D docking modes between AP and HSA. For the 2D mode, only important interacting residues are shown and represented as sticks. The hit compound is shown in pink. Residues involved in hydrogen bonding, charge, and polar interactions are represented by magenta circles. Residues involved in van der Waals interactions are represented by green circles. The solvent-accessible surfaces of atoms are represented by a blue halo around the atom. The diameter of the circle is proportional to the solvent accessible surface. Hydrogen bonding interactions with amino acid side chains are represented by a blue dash with the arrows directed toward the electron donor.

120x85mm (300 x 300 DPI)

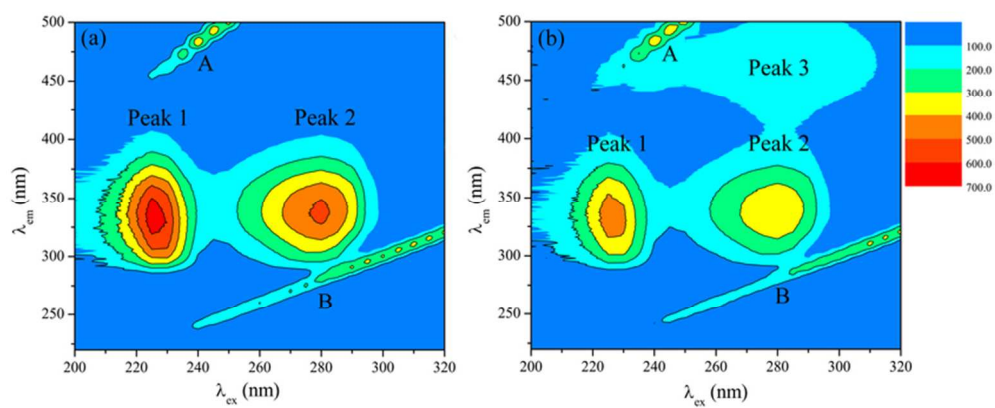


Fig. 9. Contour spectra of (a) HSA and (b) HSA-AP system in Tris-HCl buffer of pH 7.40.  $C(\text{HSA}) = 2.0 \mu\text{M}$  and  $C(\text{AP}) = 8 \mu\text{M}$ .  
71x30mm (300 x 300 DPI)

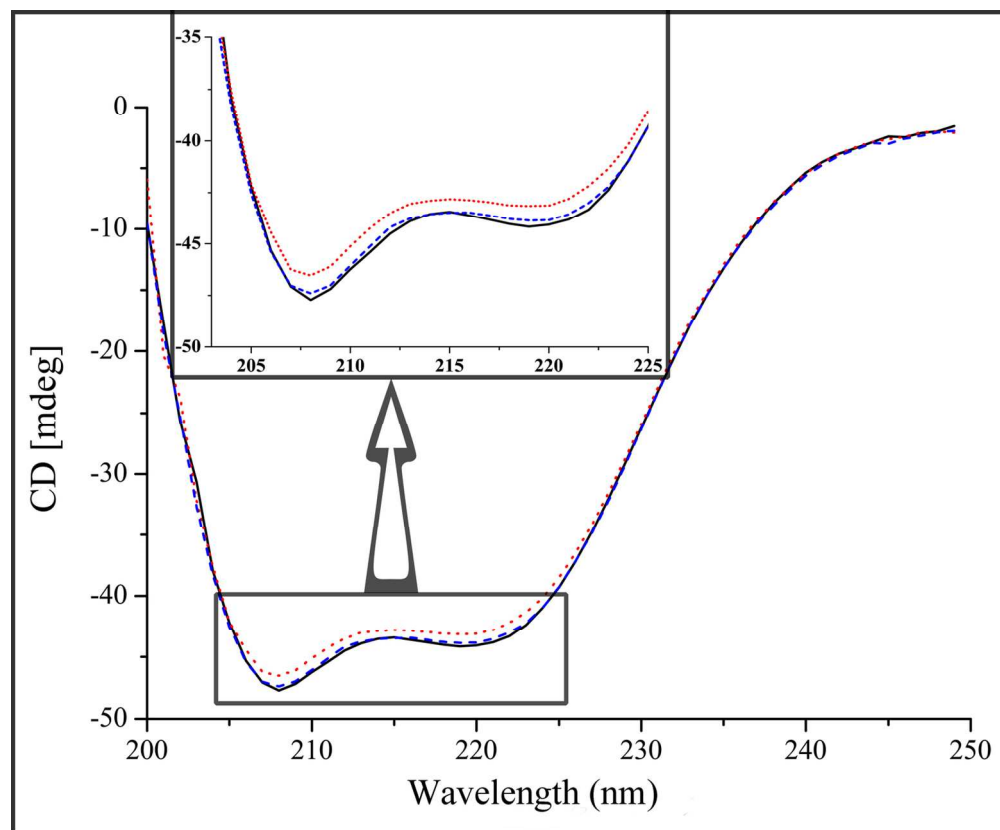
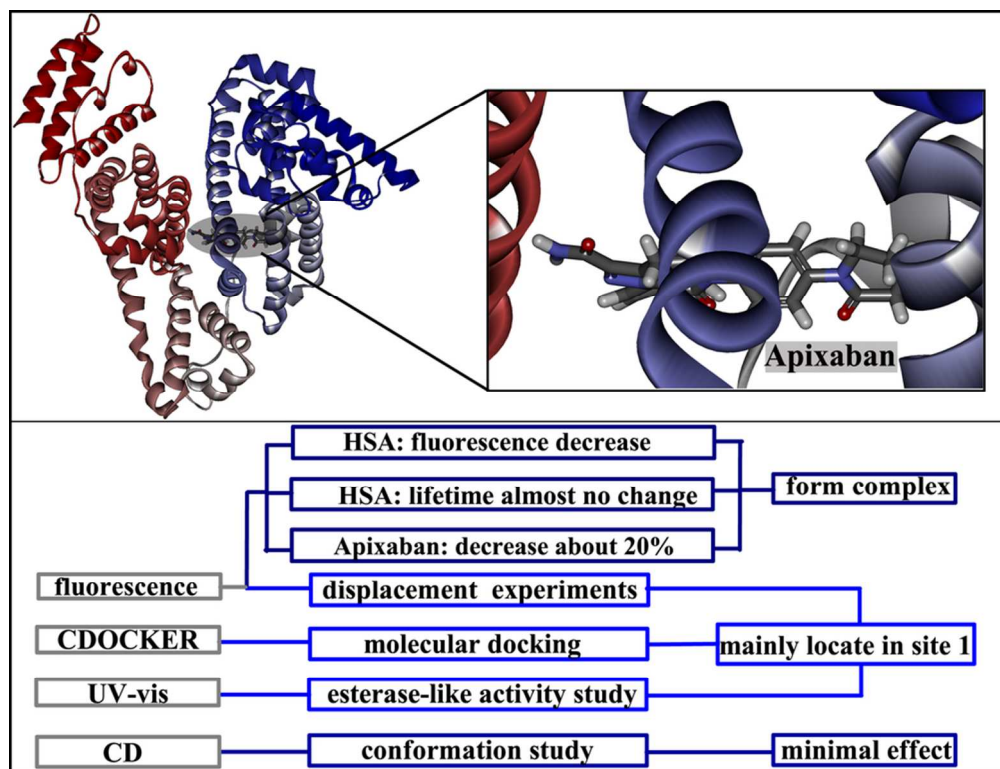


Fig. 10. Circular dichroism (CD) spectra of free HSA (2  $\mu$ M) and the HSA complex with AP ( $r_i = [\text{HSA}]/[\text{AP}] = 1:2, 1:8$ ) at pH 7.40.  
68x56mm (600 x 600 DPI)



Graphical abstract: Probing apixaban binding to human serum albumin: combining spectroscopic methods and docking investigations.  
85x64mm (300 x 300 DPI)